Evaluation of an ARPS-Based Canopy Flow Modeling System for use in Future Operational Smoke Prediction Efforts

M. T. Kiefer[1], S. Zhong[1], W. E. Heilman[2], J. J. Charney[2], and X. Bian[2]

M. T. Kiefer, Department of Geography, Michigan State University, 1407 S. Harrison Road, Room 220, East Lansing, MI, 48823, USA. (mtkiefer@msu.edu)

[1]Department of Geography, Michigan State University, East Lansing, Michigan, USA.

[2]USDA Forest Service, Northern Research Station, East Lansing, Michigan, USA.

This article has been accepted for publication and undergone full peer review but has not been through the copyediting, typesetting, pagination and proofreading process, which may lead to differences between this version and the Version of Record. Please cite this article as doi: 10.1002/jgrd.50491

©2013 This article is protected by copyright. All Rights Reserved.

Accepted Article

Abstract. Efforts to develop a canopy flow modeling system based on the Advanced Regional Prediction System (ARPS) model are discussed. The standard version of ARPS is modified to account for the effect of drag forces on mean and turbulent flow through a vegetation canopy, via production and sink terms in the momentum and subgrid-scale (SGS) turbulent kinetic energy (TKE) equations. Additionally, a downward decaying net radiation profile inside the canopy is used to account for the attenuation of net radiation by vegetation elements. As a critical step in the model development process, simulations performed with the new canopy model, termed ARPS-CANOPY, are examined and compared to observations from the Canopy Horizontal Array Turbulence Study (CHATS) experiment. Comparisons of mean and turbulent flow properties in a statistically homogeneous atmosphere are presented for two cases, one when the trees are dormant without leaves and another when the trees are full of mature leaves. The model is shown to reproduce the shape of the vertical profiles of mean wind, temperature and TKE observed during the CHATS experiment, with errors generally smaller in the afternoon and in the case with stronger mean flow. Sensitivity experiments with relatively coarse (90-m) horizontal grid spacing retain the overall mean profile shapes and diurnal trends seen in the finer-resolution simulations. The work described herein is part of a larger effort to develop predictive tools for close-range (on the order of 1 km from the source) smoke dispersion from low-intensity fires within forested areas.

Accepted Article

©2013 This article is protected by copyright. All Rights Reserved.

1. Introduction

Smoke dispersion from wildland fires is a critical health and safety issue, impacting air quality and visibility across a broad range of space and time scales. Predicting the dispersion of smoke from low-intensity fires is challenging due to the fact that it is sensitive to factors such as near-surface meteorological conditions, local topography, vegetation, and atmospheric turbulence within and above vegetation layers. Existing integrated smoke dispersion modeling systems (e.g., BlueSky [*Larkin et al.*, 2009]), which are designed for predictions of smoke from multiple sources on a regional scale, cannot resolve the processes necessary to simulate the local dispersion of smoke from low-intensity fires that can meander around the source and reside within forest canopies for an extended period of time. Simple dispersion models (e.g., SASEM, VSMOKE [*Riebau et al.*, 1988; *Lavdas*, 1996]), which typically are location specific, are often limited by the simplifying assumptions they employ to account for emissions source, topography, canopy, and the atmospheric conditions.

In order to simulate smoke dispersion within a forest canopy (defined in the context of this study as the entire vegetation layer, including the crown) and the possible transport of smoke through the canopy-atmosphere interface and into the planetary boundary layer, it is essential that the atmospheric numerical model utilized for this purpose include a canopy parameterization. Atmospheric modeling of canopy flows may be accomplished via one of two general modeling approaches: large-eddy simulation (LES) or Reynolds-averaged Navier-Stokes (RANS) modeling. With LES, large-eddy turbulent motions are explicitly predicted and unresolved fine-scale turbulent motions are parameterized, the

Accepted Article

©2013 This article is protected by copyright. All Rights Reserved.

latter typically referred to as subgrid-scale (SGS) or subfilter-scale motions. The fundamental premise of LES is that the filter scale, which separates resolved motions from SGS motions, lies in the inertial sub-range of the turbulence spectrum [for a review of the LES approach see *Mason*, 1994]. In contrast, use of RANS implies that only the mean component of flow is explicitly resolved, while the effect of correlations of fluctuating quantities on the resolved mean flow are parameterized. Examples of canopy flow studies using LES include *Shaw and Schumann* [1992], *Dwyer et al.* [1997], *Watanabe* [2004], and *Dupont and Brunet* [2008], while studies utilizing RANS include *Wilson and Shaw* [1977], *Yamada* [1982], *Ayotte et al.* [1999], and *Ross and Vosper* [2005].

In this manuscript, we describe the development of an integrated canopy flow modeling system, based on the Advanced Regional Prediction System (ARPS) [*Xue et al.*, 2000, 2003] version 5.2.12. ARPS is a three-dimensional, compressible, nonhydrostatic atmospheric model with a terrain-following coordinate system. ARPS is designed to simulate microscale- through regional-scale flows, and has been validated extensively in the last two decades [e.g., *Xue et al.*, 2000, 2001]. However, the standard ARPS formulation lacks the capability to simulate atmospheric variables (e.g., wind velocity, temperature) within a multi-layer canopy. In the ARPS framework, as with many mesoscale models, the bulk effect of a vegetation canopy on the atmosphere is computed at the surface (skin) level, beneath the lowest model grid point. A modified version of ARPS has been developed by *Dupont and Brunet* [2008] that accounts for the effects of vegetation elements on flow through a multi-layer canopy. However, application of their version of ARPS is limited to modeling neutral boundary layers since no attempt was made to include a canopy heat source/sink or to modify the surface energy budget. The need for a modeling system

Accepted Article

©2013 This article is protected by copyright. All Rights Reserved.

capable of simulating mean and turbulent components of flow through a canopy under all stability regimes, including regimes locally modified by wildland fires, motivated the development of a new canopy-flow modeling system, termed ARPS-CANOPY.

Note that while there is ample evidence in the literature to suggest that RANS can be successfully applied to canopy flows, the lack of any resolved turbulence makes it a less attractive option for smoke dispersion modeling. Furthermore, while ARPS can be run in both RANS mode [at scales O(1km) or larger] or LES mode [at scales O(10 m) or smaller], the need to apply the model in near-real time mode for potential operational smoke dispersion prediction efforts means that a hybrid approach is needed. Thus we intend to assess the performance of ARPS-CANOPY, run with grid dimensions that neither preclude the explicit resolution of turbulent motions, nor guarantee that the bulk of TKE is contained within the resolved turbulent motions (i.e., not true LES). In this study we evaluate ARPS-CANOPY in a fire-free and smoke-free environment. However, our choice of modeling approach is consistent with our overarching hypothesis that the ability to resolve some scales of turbulence and explicitly resolve some atmospheric processes relevant to smoke dispersion from low-intensity fires will lead to more accurate smoke predictions than a RANS-based approach.

The remainder of this paper is organized as follows. A description of the standard ARPS model and the canopy modifications made in ARPS-CANOPY is presented in Section 2, followed by a summary of the observational data set used to evaluate ARPS-CANOPY, the Canopy Horizontal Array Turbulence Study (CHATS) [*Patton et al.*, 2011; *Dupont and Patton*, 2012a, b], in Section 3. Subsequently, a description of the model configuration and parameterization options chosen for the model assessment simulations is provided in

Accepted Article

©2013 This article is protected by copyright. All Rights Reserved.

Section 4, results from the simulations are presented in Sections 5.1 and 5.2, and results from a series of grid structure sensitivity experiments are discussed in Section 5.3. Finally, the paper is concluded in Section 6.

2. Model Description

2.1. Modifications made to ARPS: Canopy flow parameterization

Simulation of flow inside a canopy requires that one account for the effects of the canopy on air flow. Canopies alter flow in the following ways [*Wilson and Shaw*, 1977]: loss of momentum due to aerodynamic drag; conversion of mean flow kinetic energy into turbulent kinetic energy (TKE) in the wakes downwind of vegetation elements; break-down of large-scale turbulent eddies into small-scale turbulent motions in the wakes downwind of vegetation elements; and buoyant production/destruction of TKE through warming/cooling of the canopy air space. In order to account for the aggregate effect of leaves, branches, and other small obstructions to air flow in a grid volume, the most common approach taken for numerical modeling of canopy flows involves addition of a drag force term to the momentum equation and the addition of a sink term to the SGS TKE equation to account for the enhanced dissipation of TKE due to the interaction of flow with canopy elements [e.g., *Dupont and Brunet*, 2008]. However, it is not clear that a sufficient gap exists in the turbulence spectrum between the relatively small wake-scale eddies and the relatively large SGS motions for the production of TKE at wake scales to be considered a sink of SGS TKE. *Kanda and Hino* [1994] recommend that both a production and sink term be included in the SGS TKE equation, while more recent work by *Shaw and Patton* [2003] suggests that only a sink term is needed.

Accepted Article

©2013 This article is protected by copyright. All Rights Reserved.

Based on this review of canopy flow modeling methods, the standard ARPS model has been modified accordingly; we begin with a discussion of modifications made to the momentum equation. Using Einstein summation convention and written in Cartesian coordinates for a dry atmosphere over flat terrain, the momentum equation in ARPS-CANOPY may be expressed as

$$\bar{\rho}\left(\frac{\partial \tilde{u}_i}{\partial t}+\tilde{u}_j\frac{\partial \tilde{u}_i}{\partial x_j}\right)=-\frac{\partial}{\partial x_i}\left(\tilde{p}'-\alpha_{div}\frac{\partial \bar{\rho}\tilde{u}_j}{\partial x_j}\right)-2\bar{\rho}\omega_j\epsilon_{ijk}\left(\tilde{u}_k-\overline{u_k}\right)-\bar{\rho}g\left(\frac{\tilde{\theta}'}{\bar{\theta}}-\frac{\tilde{p}'}{\bar{p}c_s^2}\right)\delta_{i3} - \frac{\partial \tau_{ij}}{\partial x_j}-\eta\bar{\rho}C_dA_p\tilde{V}\tilde{u}_i \quad (1)$$

where the overtilde indicates grid volume-averaged variables. In this equation, t is time, $u_i(u_1=u, u_2=v, u_3=w)$ is the instantaneous velocity component along $x_i(x_1=x, x_2=y, x_3=z)$, $\bar{\rho}$ is the base state air density, p is air pressure, g is the acceleration due to gravity, and θ is potential temperature. Furthermore, δ_{ij} is the Kronecker delta, ϵ_{ijk} the alternating unit tensor, α_{div} a damping coefficient intended to damp acoustic waves, ω_j is the angular velocity of the earth, and c_s is the speed of sound. Variables with prime notation denote deviations from a horizontally homogeneous, time invariant base state, the latter indicated by an over-bar.

The terms on the right-hand side of Eq. (1) represent, respectively, the pressure-gradient force term, the Coriolis term, the buoyancy term, the turbulent mixing term, and the drag force term associated with the canopy vegetation. Note that as in standard ARPS, the Reynolds or sub-grid scale stress tensor, τ_{ij} is modeled through a SGS gradient transport approach, computed as a function of eddy viscosity (ν_t), itself modeled as the product of

©2013 This article is protected by copyright. All Rights Reserved.

a stability-dependent length scale and velocity scale [square-root of SGS TKE (e)]. For more details, the reader is referred to *Xue et al.* [2000].

Following *Dupont and Brunet* [2008], we have added a canopy drag term [last term in Eq. (1)] to the standard ARPS momentum equation to account for drag that occurs due to the presence of the canopy elements. In the canopy drag term, C_d is the mean drag coefficient of the canopy and A_p (m^2 m^{-3}) is the plant area density of the vegetation, defined as the one-sided area of all plant material. The magnitude of the resolved-scale velocity, V, is defined as $V = (u^2 + v^2 + w^2)^{\frac{1}{2}}$. A modification has been made to the original term presented in *Dupont and Brunet* [2008] in that a factor of η is included to incorporate effects of vegetation fraction less than unity, following the work of *Yamada* [1982] and *Sun et al.* [2006]. We have introduced η, a parameter that represents the fraction of a grid cell covered by trees, to account for the fact that ARPS-CANOPY is designed to be run with grid cells large enough that an assumption of land-cover homogeneity across the grid cell is not necessarily appropriate. The A_p profile is considered to be representative of the canopy density within the vegetated portion of each grid cell. As an example, consider a grid cell in which trees are assumed to cover 80% of the ground, and the remaining 20% of the grid cell is open. Applying the factor of η to Eq. (1) results in a drag term that is 20% smaller than it would be if grid cell homogeneity was assumed, since 20% of the grid cell is specified as non-vegetated and is therefore absent of canopy drag. This method does not account for heterogeneous aggregation of trees, a fact that should be kept in mind when interpreting results. The factor η is included in all canopy terms (see below).

Before proceeding, some comment on the use of a constant drag coefficient is in order. Although ARPS-CANOPY uses a constant canopy drag coefficient, it is worth noting

©2013 This article is protected by copyright. All Rights Reserved.

that some canopy models utilize a drag coefficient that varies with vegetation element Reynolds number [e.g., *Shaw and Patton*, 2003; *Froelich et al.*, 2011]. *Shaw and Patton* [2003] argue that use of a constant coefficient renders the drag term essentially a pressure drag term, and addition of a Reynolds-number-sensitive drag coefficient is necessary for proper parameterization of viscous drag. However, we choose here to follow *Dupont and Brunet* [2008] and use a constant coefficient (C_d=0.2), while acknowledging that in reality C_d may decrease as wind speeds increase due to streamlining effects [*Rudnicki et al.*, 2004], and conversely, C_d may increase as wind speeds decrease due to the greater role of molecular viscosity at weak wind speeds. It is worth noting that while use of a constant drag coefficient is a simplification of a complex process, it is not without precedent, having been applied to canopies with a wide range of canopy densities [e.g., *Shaw and Schumann*, 1992; *Pinard and Wilson*, 2001; *Watanabe*, 2004; *Sun et al.*, 2006; *Dupont and Brunet*, 2008].

The conservation equation for SGS TKE (e) in ARPS-CANOPY may be expressed as:

$$\frac{\partial e}{\partial t} + \tilde{u}_j \frac{\partial e}{\partial x_j} = -\tau_{ij}\frac{\partial \tilde{u}_i}{\partial x_j} - \frac{g}{\bar{\theta}}\tau_{i\theta}\delta_{i3} + \frac{\partial}{\partial x_j}\left(2\nu_t \frac{\partial e}{\partial x_j}\right) - C_\epsilon \frac{e^{3/2}}{l} - 2\eta C_d A_p \tilde{V} e + \beta \eta C_d A_p \tilde{V}^3 \tag{2}$$

where the terms on the right hand side of Eq. (2) represent, respectively, shear production, buoyancy prodution/destruction, turbulent transport, dissipation, canopy drag force sink, and canopy wake production. In Eq. (2), $\tau_{i\theta}$ is the subgrid-scale heat flux, l is a dissipation length scale, and C_ϵ is a dissipation constant. For more details, the reader is referred to *Xue et al.* [2000].

©2013 This article is protected by copyright. All Rights Reserved.

The second to last term in Eq. (2) was added following *Dupont and Brunet* [2008] in order to account for the loss of SGS TKE to both heat and very small (and thus dissipative) wake-scale eddies, a process often referred to as a "short-circuit" of the inertial eddy cascade [*Raupach and Thom*, 1981; *Finnigan*, 2000]. Following *Kanda and Hino* [1994], we have also added a production term to the SGS TKE equation [last term in Eq. (2)] to represent the production of SGS TKE in the wakes of canopy elements, at scales large enough that the turbulence does not dissipate immediately yet small enough that it remains unresolved. The coefficient β represents the fraction of kinetic energy lost due to canopy drag that contributes to wake production in SGS flow. A value of 0 means that no kinetic energy lost from the resolved-scale flow due to canopy drag transfers to wake-scale turbulence (i.e., energy is lost to heat only), whereas a value of 1 means that all kinetic energy lost from the resolved-scale flow due to canopy drag goes to the production of wake-scale turbulence. Favoring a conservative approach, we set β equal to 0.1 for all simulations [*Kanda and Hino*, 1994]. Examination of the sensitivity of mean and turbulent flow in ARPS-CANOPY to β is left to future work.

2.2. Modifications made to ARPS: Canopy heat source parameterization

Modeling the evolution of air temperature within a forest canopy is essential for modeling buoyancy effects on flow through a canopy. Thus, various studies have considered how best to simulate canopy element heating/cooling and the heating/cooling of adjacent air within the vegetation canopy. The models used in these studies may be classified into three categories, those that explicitly simulate the radiative transfer between adjacent cells or volumes of canopy [e.g., *Budagovskii et al.*, 1968; *Kimes et al.*, 1981; *Smith et al.*, 1981, 1997; *Froelich et al.*, 2011], those that consider the radiative balance of a canopy

©2013 This article is protected by copyright. All Rights Reserved.

element rather than a volume or grid cell [i.e., radiosity models; *Borel et al.*, 1991; *Chelle and Andrieu*, 1998], and those that prescribe a downward-decaying profile of net radiation (or alternatively, heat flux) within the canopy to account for the heating/cooling of vegetation elements [e.g., *Yamada*, 1982; *Shaw and Schumann*, 1992; *Shen and Leclerc*, 1997; *Sun et al.*, 2006].

The latter method, first proposed by *Uchijima* [1961], involves specification of a net radiation profile that decays downward from canopy top as a function of the cumulative leaf area index (computed from the top of the canopy downward) and an empirically determined extinction coefficient. Thus, net radiation need only be computed in the model at the top of the canopy, eliminating the computational expense of explicitly modeling radiative transfer at each level within the canopy. The heat contribution from the canopy elements to the air is then computed via the vertical divergence of net radiation, with the horizontal divergence of net radiation typically neglected. In the absence of a radiation parameterization, one may choose to specify a heat flux profile to account for canopy heating/cooling [e.g., *Shaw and Schumann*, 1992].

While each of the methods have been applied extensively and shown to be robust [e.g., *Sun et al.*, 2006; *Froelich et al.*, 2011], we adopt in this study the net radiation profile method [*Sun et al.*, 2006] due to it's relative simplicity. Thus, we follow *Sun et al.* [2006] and compute net radiation flux at canopy top (at height h) as

$$R_{Nh} = (1 - \alpha_t)\, S + \varepsilon_c \left(R_{Lh} \downarrow - R_{Lh} \uparrow\right) \tag{3}$$

where α_t is the canopy albedo, S represents the incoming solar radiation flux intercepting the top of the canopy, ε_c is canopy emissivity, and $R_{Lh} \uparrow$ and $R_{Lh} \downarrow$ are upward and

©2013 This article is protected by copyright. All Rights Reserved.

downward longwave radiation. The formulation of Eq. (3) is otherwise identical to the standard ARPS ground radiation budget, except that here we use a constant value of albedo appropriate for forested areas, and the outgoing longwave component ($R_{Lh} \uparrow$) is computed as a function of air temperature at canopy top, rather than skin temperature. Specification of canopy heating parameters (e.g., α_t) in Eq. (3) and subsequent equations is discussed in Section 4.2.

Following *Sun et al.* [2006], we have also prescribed a profile of net radiation that produces an approximately exponential decay within the canopy,

$$R_{Np}(z) = R_{Nh}\left[exp\left\{-kP_L(z)\right\} - \eta\left(1 - \frac{z}{h}\right) exp\left\{-kP_L(0)\right\}\right] \tag{4}$$

In Eq. (4), k is an extinction coefficient, and $P_L(z) = \int_z^h A_p(z)dz$ is the local plant area index (PAI), which indicates the plant area per unit horizontal area of the canopy above height z. Equation (4) states that the transmission of net radiation through a vegetation canopy exhibits an approximately exponential decay with increasing penetration depth into the canopy, as a function of the local PAI.

The time rate of change of potential temperature due to the heat source/sink within the canopy is computed as:

$$\frac{\partial\theta}{\partial t} = \frac{(1-\eta)}{\rho_a C_p}\frac{\partial R_N}{\partial z} + \frac{\eta}{\rho_a C_p + \rho_c C_c}\left(1 + \frac{1}{B}\right)^{-1}\frac{\partial R_{Np}}{\partial z} \tag{5}$$

where θ is the potential temperature of the air and R_N is the net radiation flux within the clearing fraction of each grid box. Equation (5) states that the time rate of change of potential temperature inside the canopy is computed as the weighted sum of vertical radiation flux divergence in the clearing fraction of each grid cell, and vertical radiation flux

©2013 This article is protected by copyright. All Rights Reserved.

divergence in the vegetated part of each grid cell. The leading factor in the second term on the right hand side of Eq. (5) accounts for heat storage in the canopy elements (through the canopy element volumetric heat capacity, $\rho_c C_c$), as well as partitioning of energy into sensible and latent heat flux (through the Bowen ratio, B). In ARPS-CANOPY, as in *Sun et al.* [2006], a constant value of B is specified in each simulation (see Section 4.2 for more details); thus, there is no parameterization of canopy resistance in the model.

At this point, a word of caution is required regarding the canopy heat source we have added to ARPS. Since we follow *Sun et al.* [2006], our model assumes that the rate of heating/cooling of vegetation elements is identical to that of adjacent canopy air spaces. *Froelich et al.* [2011] argue that such an assumption is not acceptable, with the largest error occurring near sunrise (sunset) when canopy elements warm (cool) rapidly through radiative gain (loss), and air temperature changes lag behind. As *Froelich et al.* [2011] assert, *Sun et al.* [2006] unintentionally simulated different rates of heating/cooling for canopy elements and canopy air spaces due to the abnormally large value of local canopy density [ρ_c in Eq. (5)] utilized in their study (as large as 9.1 kg m^{-3}). In ARPS-CANOPY, we compute ρ_c as $[(C_{D_m} + C_{M_m})\, A_p(z)]_{leaf-off}$, which is interpreted as the total mass (sum of dry canopy mass and mass of moisture in canopy) per unit ground area multiplied by the plant area density at each grid level in the canopy. This follows from *Sun et al.* [2006], except that we opt to neglect the impact of leaves on local canopy density, since leaves make up a small proportion of canopy mass compared to branches [*Garai et al.*, 2010]. This method yields local canopy density values that are at least an order of magnitude smaller than *Sun et al.* [2006] and more in line with what *Froelich et al.* [2011] recommend. It is important, however, to emphasize that an accepted method of parameterizing local

©2013 This article is protected by copyright. All Rights Reserved.

canopy density does not exist at this time. Note that differences between canopy element and air temperature rates of change are likely to be smallest during the daytime, the period of time which is the primary focus of our study.

Lastly, the net radiation budget at the ground is given by:

$$R_{NG} = \eta R_{Nh} exp\left[-kP_L(0)\right] + (1-\eta)\left[(1-\alpha_G)\,S + \varepsilon_G\left(R_{LG}\downarrow - R_{LG}\uparrow\right)\right] \tag{6}$$

where symbols with subscript "G" refer to ground surface equivalents of the canopy top parameters in Eq. (3), and $P_L(0)$ is local PAI computed at the ground (i.e., total PAI). Note that Eq. (6) is used by the land surface model as part of the integration of skin temperature whereas the net radiation flux in Eq. (4) is used to compute the canopy source term in the thermodynamic equation [Eq. (5)].

3. CHATS Experiment Overview

In this study, we evaluate ARPS-CANOPY by comparing simulated wind and temperature to observations taken during the CHATS field experiment. CHATS was conducted within a deciduous walnut orchard near Dixon, California from 15 March to 12 June 2007, and consisted of three phases: (I) pre leaf-out (15 March - 13 April), (II) post leaf-out (13 May - 12 June), and (III) transitional (14 April - 12 May). Here we define pre leaf-out as the period during which the trees were bare, i.e. the trees were dormant without leaves; and post leaf-out as the period during which the trees had full coverage of mature leaves. The trees in the section of orchard with CHATS instrumentation were planted in a grid pattern with approximately 7 m between each row/column of trees as measured at trunk height. The horizontal distribution of trees was nearly homogeneous, with an average tree height of 10 m and average tree age of 25 years.

©2013 This article is protected by copyright. All Rights Reserved.

Accepted Article

A variety of instrumentation was utilized during the experiment, including a horizontal array of fast-response instrumentation, a 30-meter instrumented tower, and a mini sodar/RASS (Radio Acoustic Sounding System) sited outside of the orchard. The 30-meter tower was instrumented with sonic anemometers, hygrothermometers, hygrometers and hot film anemometers, with various combinations of instrumentation mounted at 13 fixed levels: 1.5, 3, 4.5, 6, 7.5, 9, 10, 11, 12.5, 14, 18, 23 and 29 m above ground level (AGL). Sonic anemometers, measuring the three wind components and virtual temperature at 60 Hz frequency, and aspirated hygrothermometers measuring mean temperature and relative humidity at 2 Hz frequency, were instrumented at each level. Additionally, pyranometers and pyrgeometers were deployed at 16 m AGL to measure the broad spectrum up-welling and down-welling above-canopy radiation, with a similar setup beneath the canopy at 2 m AGL. Furthermore, a net radiometer was installed at 2 m AGL to complement the 4-component radiation measurements. For a detailed description of the field experiment, including additional instrumentation not addressed in this paper, see *Patton et al.* [2011].

The evaluation of ARPS-CANOPY is performed by comparing temporally-averaged model output to temporally-averaged sonic anemometer and hygrothermometer data from the instrumented tower. Although longer period averages are used in the model evaluation, the processing of data begins with 30-minute block averages. Moreover, while the CHATS data were sampled at much higher frequencies, only 5-minute averaged quality-controlled statistics were available for this study. In the case of mean quantities (e.g., mean wind speed), a simple arithmetic average of six 5-minute mean values yields the desired 30-minute mean quantity. However, in order to compute 30-minute mean covariances (or variances) from the 5-minute mean statistics, we use the following formula:

©2013 This article is protected by copyright. All Rights Reserved.

$$\overline{x\prime y\prime}^N = \frac{1}{m}\sum_{j=1}^{m}\left(\overline{x\prime y\prime}^{N_j} + \overline{X}^{N_j}\overline{Y}^{N_j}\right) - \frac{1}{m}\sum_{j=1}^{m}\overline{X}^{N_j}\frac{1}{m}\sum_{j=1}^{m}\overline{Y}^{N_j} \tag{7}$$

In this formula, $X(t)$ and $Y(t)$ are two time series that are expanded into mean and perturbation as $X(t) = \overline{X} + x\prime(t)$ and $Y(t) = \overline{Y} + y\prime(t)$, N is an averaging period (in this case, 30 minutes), N_j is an averaging period shorter than N (in this case, 5 minutes), and there are m segments of length N_j in period N. Finally, all covariances and means (both model and observations) are averaged over three-hour blocks for a general assessment of diurnal evolution (Section 5.1).

For the purposes of the model assessment, two cases are considered, one pre leaf-out (29 March) and one post leaf-out (20 May). The cases were chosen based on a review of satellite and other meteorological data (e.g., surface maps, upper-air charts) to identify days with clear skies and an absence of synoptic or mesoscale phenomena in the region, such as fronts or mountain-valley flows. Logs of experiment activity were also examined to ensure that no instrument maintenance or irrigation of the orchards was conducted on the days of interest. Figure 1 presents profiles of plant area density for the two cases, measured with a Li-Cor LAI-2000, averaged over measurements taken throughout each period, and interpolated to the ARPS-CANOPY model grid (see Section 4.1); recall that plant area density is defined as the one-sided area of all plant material (e.g., leaves, branches), per unit volume of canopy. Note that PAI, defined earlier as the vertically integrated plant area density, is approximately 0.75 (2.75) for the pre (post) leaf-out case.

Accepted Article

©2013 This article is protected by copyright. All Rights Reserved.

4. Model Configuration and Parameterization

4.1. Numerical Design

We now outline the configuration of the ARPS-CANOPY simulations. A 1-way nesting procedure is utilized with two three-dimensional computational domains, and a periodic boundary condition applied at the lateral boundaries of the outer domain. For simplicity, the inner domain is centered within the outer domain. Both domains consist of 83 x 83 x 83 grid points (including points used only for boundary condition calculations), with horizontal grid spacing of 90 m (30 m) applied in the outer (inner) domain. Vertical grid spacing of 2 m is utilized in both domains, up to a height of 84 m, above which vertical stretching is applied. With this vertical grid structure, there are 5 grid points at or below the canopy crown (canopy height is 10 m). The use of 2-m grid spacing represents a compromise between the need for sufficiently small vertical grid spacing with which to resolve strong vertical gradients in wind and temperature near canopy top, and the need to restrain computational expense. The top of both model domains is at 12 km, with a rigid lid upper boundary condition and a Rayleigh damping layer in the uppermost 2 km, to prevent reflection of waves from the upper boundary. The bottom boundary is treated as a rigid surface, with surface momentum and heat fluxes computed via bulk aerodynamic drag formulas, as in the standard ARPS model. All simulations are initialized at 0400 Local Standard Time (LST: UTC-8) and run for a total of 12 hours.

For all simulations, ARPS-CANOPY is initialized with a horizontally homogeneous atmosphere with velocity fluctuations set to zero at every grid point at time zero (0400 LST). However, a random initial perturbation (of magnitude 1 K) is applied to the surface potential temperature field at the initial time to promote the development of 3D turbulent

Accepted Article

©2013 This article is protected by copyright. All Rights Reserved.

structures. In order to simulate the atmosphere to a height of 12 km AGL, soundings were generated by first interpolating 32-km resolution North American Regional Reanalysis (NARR) data [*Mesinger et al.*, 2006] at the tower location (38.488 N ; 121.846 W). Subsequent to the NARR interpolation, quality-controlled wind data from the nearby Sacramento, CA wind profiler (approximately 40 km southeast of the 30-m tower), wind speed data from the mini-Sodar (data are generally available every 20 m from 40 to 300 m AGL) and wind speed and direction data from the 30-m tower were substituted for the NARR values in the lower atmosphere. Note that mini-Sodar wind speed data at a given height was rejected if the signal to noise ratio was less than zero, or if error codes exceeded a given threshold (W. Brown, personal communication). Wind direction data from the sodar and temperature data from the RASS were omitted from the process due to poor agreement with both the tower and NARR data, and generally unreliable behavior. Finally, manual smoothing was applied to the initial state profiles to ensure smooth transitions between the NARR, profiler, sodar, and tower data. Figure 2 illustrates both the domain-deep initial state, as well as the initial temperature and wind speed profiles in the lowest 30 m of the model atmosphere. Lastly, initial state soil temperature was derived from 30-min averaged observed values and soil heat capacity was determined from 3-hourly measurements.

4.2. Parameterizations

A 1.5-order SGS turbulence closure scheme with a prognostic equation for TKE is utilized, with the addition of canopy source and sink terms [Eq. (2)]. The standard ARPS anisotropic turbulence option is used in which both horizontal and vertical components of eddy viscosity are computed; this option is recommended when vertical grid spacing

©2013 This article is protected by copyright. All Rights Reserved.

Accepted Article

is considerably smaller than horizontal grid spacing [*Xue et al.*, 2000]. Possible impacts of grid structure on simulations of mean and turbulent flow are discussed in Section 5.3. We wish to point out that the turbulence closure we utilize here has been tested extensively and has been found to produce the correct vertical structure of mean variables and turbulent statistics in the absence of a forest canopy (not shown). The standard ARPS two-layer force-restore land surface model based on *Noilhan and Planton* [1989] and *Pleim and Xiu* [1995] is used, with one subtle but important distinction. ARPS is typically applied to mesoscale or larger flows, and thus the lowest model grid level is usually located above the top of the vegetation (e.g., grasses, trees). In this study, our use of 2-m vertical grid spacing with a 10-m tall canopy means that the lowest grid level (1 m AGL) is well below the top of the orchard canopy. To avoid "double-counting" due to the use of both a land surface model (which itself is designed to take into account the effect of vegetation below the lowest model level) and an explicit canopy drag term in the momentum equation, an assumption of sparse grasses is made in all simulations, and we specify a uniform ground surface drag coefficient of $3\text{x}10^{-3}$. Note that two separate drag coefficients are applied in the model, a canopy drag coefficient applied inside the vegetation canopy [C_d in Eq. (1)] and a surface drag coefficient utilized for surface flux calculations.

Consistent with the standard ARPS formulation, shortwave and longwave radiation components in the atmosphere and at the ground are computed following *Chou* [1990, 1992] and *Chou and Suarez* [1994], however with computation of the canopy source term and attenuation of net radiation inside the canopy applied as discussed in Section

Accepted Article

©2013 This article is protected by copyright. All Rights Reserved.

2.2. Moist processes are neglected, and the Coriolis force is computed (as a function of central latitude only) in all simulations.

Regarding canopy parameters in Eqs. (3) - (6), we use the following for simulations of the CHATS canopy. The canopy albedo, α_t, canopy emissivity, ε_c, and extinction coefficient, k, are assumed to be uniform across the orchard and are set to 0.1, 0.98, and 0.6, respectively [as in *Sun et al.*, 2006]. Furthermore, we use values of canopy mass per unit area ($C_{D_m} + C_{M_m}$) equal to 4.21 kg m^{-2}, while setting specific heat capacity of the canopy elements (C_c) to 2760 J kg^{-1} K^{-1}. These values were utilized by *Garai et al.* [2010] as part of biomass heat storage analysis inside the CHATS orchard. For Bowen ratio (B), we use mean values of 0.35 for leaf-on conditions and 1.5 for leaf-off conditions, based on CHATS observed fluxes at canopy top. Note that albedo values derived from CHATS observed radiation components average around 0.15 and are comparable for pre and post leaf-out conditions (not shown); thus insomuch as the present simulations are concerned, more solar radiation enters the canopy in the ARPS-CANOPY simulations than in reality, a fact that must be kept in mind when evaluating results. As will be discussed later, model errors in wind, temperature, and TKE may be attributed to the use of time-invariant values of coefficients and parameters, as variation on diurnal and seasonal timescales is neglected. Lastly, regarding the specification of model domain vegetation fraction (η), aerial photographs of the orchard were examined to determine the approximate fraction of ground covered by trees inside the orchard. Based on this analysis, η is set to 60% and 75% for the pre and post leaf-out cases, respectively.

Accepted Article

©2013 This article is protected by copyright. All Rights Reserved.

4.3. External Forcing

We wish to provide some clarification regarding the forcing or "driving" of the ARPS-CANOPY simulations we have outlined here. It is important to keep in mind that the choice of periodic lateral boundary conditions for the outer grid implies that no large-scale influence (e.g., pressure gradient forcing) is exerted on the atmosphere in our simulations, outside of any large-scale information contained in the initial (base state) profile. The flow is driven by the geostrophic pressure gradient associated with the time-invariant base-state wind [*Dupont and Brunet*, 2008]. Therefore, temporal variations in wind speed in the simulations cannot be attributed to an evolving large-scale pressure gradient, since no external information is provided at the boundaries. Furthermore, the components of radiation intercepting the canopy and ground surface [i.e., Eqs. (3) and (6)] are not derived from measured shortwave and longwave fluxes. Rather, the components are parameterized as described in Section 4.2. In Section 5.2, the performance of the ARPS-CANOPY radiation parameterization will be evaluated with CHATS radiation measurements. Note that we did not apply nudging methods to the predicted variables; what is presented in the figures that follow are model predictions alone. In this study, we examine the performance of the model in the absence of large-scale processes, and without observed radiation inputs or any other information that would not be available if ARPS-CANOPY were being applied to real-time prediction.

5. Results and Discussion

5.1. Model Evaluation: Mean and Turbulent Flow

In order to evaluate the ability of ARPS-CANOPY to simulate flow through a vegetation canopy, 3-hour mean wind speed, wind direction, and temperature profiles from the

©2013 This article is protected by copyright. All Rights Reserved.

inner domain simulation (30-m horizontal grid spacing) are compared to CHATS observations and the results are presented in Figs. 3 and 4. We choose to analyze 3-hour averages (as opposed to, for example, 1-hour averages) to examine broader diurnal trends without the higher frequency variability that the current numerical experiment design is not capable of reproducing with the lack of time-varying lateral boundary conditions or observed radiation inputs (see Section 4.3). It is worthwhile to point out here that although our experimental design constrains the application of ARPS-CANOPY to horizontally homogeneous canopies, with mainly diurnal variations in heat and momentum, the flexibility of ARPS-CANOPY makes it applicable to horizontally inhomogeneous flows that vary on diurnal and non-diurnal timescales.

Examining the pre leaf-out case first (Fig. 3), we see that while the model underestimates the roughness sub-layer mean wind speeds in the early-mid morning period (0400-1000 LST, Fig. 3a), it produces wind speeds within 0.5 m s^{-1} of the observed values from mid-morning onward (1000-1600 LST). In the case of wind direction (Fig. 3b), the model correctly maintains a nearly uniform profile, although prior to 1300 LST the simulated wind direction differs by approximately 20 degrees (north-northwest in the model vs. north-northeast in the observations). Examining temperature (Fig. 3c), we see that the model reproduces the observed diurnal trends and profile shapes throughout the simulation. It is evident though that the simulated temperatures are 1-1.5 ^{o}C too cold (warm) between 0400-1000 (1000-1600) LST, and the simulated temperature gradient is too strong between 1000-1600 LST.

Evaluating the post leaf-out case next (Fig. 4), we see that as with the pre leaf-out case, the overall shape of the simulated vertical wind speed profiles is similar to the observations.

©2013 This article is protected by copyright. All Rights Reserved.

The model simulation correctly depicts the very weak wind speeds inside the canopy and also exhibits wind speeds above the canopy within the observed range. However, the model does not reproduce the evolution of wind speed and direction (Figs. 4a and 4b). Wind speeds in the CHATS observations are strongest during the 0400-0700 LST and 1300-1600 LST periods and weaker in the interim periods, but the simulation exhibits the weakest wind speeds during the first period and stronger though generally steady wind speeds during the remainder of the simulation. Furthermore, the diurnal variation of wind direction in the simulations is smaller than what was observed. However, these model wind errors must be put in the proper context; the simulations are run in idealized mode without the benefit of larger-scale information (e.g., mesoscale variability; Section 4.3), and mean wind speeds are less than 2.5 m s^{-1} at all times.

In spite of the model errors, it is worth noting that the model is able to reproduce a kinked wind direction profile inside the canopy during the morning (note the complete absence of this feature in the pre leaf-out observations and simulations). *Dupont and Brunet* [2008] attribute such a swing in wind direction inside the canopy to an indirect Coriolis effect wherein weak shear stress within the canopy causes the wind to turn and align with the large-scale pressure gradient. However, caution must be exercised in attributing the wind direction variation in the CHATS orchard to a particular process since wind speeds inside the canopy are small (less than 0.5 m s^{-1}). Regarding temperature (Fig. 4c), we see that the model is able to capture the evolution and vertical structure. While magnitudes of model error larger than the pre leaf-out case simulation are evident, the post leaf-out simulation exhibits errors opposite that of the pre leaf-out case (cf. Figs. 3c and 4c). Note that the absence of any daytime inversions inside the canopy is consistent with

Accepted Article

©2013 This article is protected by copyright. All Rights Reserved.

the relatively sparse nature of the CHATS orchard canopy. Daytime inversions within vegetation canopies develop when relatively strong heating of the atmosphere occurs in densely vegetated layers of the upper canopy, with relatively weak heating occurring beneath. While such inversions are common in denser canopies [e.g, *Andreae et al.*, 2002; *Utiyama et al.*, 2004], a review of the full CHATS dataset by *Dupont and Patton* [2012a] revealed no evidence of daytime inversions inside the orchard canopy.

The mean profile assessment has identified varying degrees of model error for each of the variables examined. The error magnitudes noted here are within the range reported in studies using contemporary canopy-parameterizing models [temperature: 1-4 C; wind: 1-2 m s^{-1}; TKE: 0-0.5 m^2 s^{-2}; see *Sogachev et al.*, 2002; *Froelich et al.*, 2011; *Aumond et al.*, 2013]. The goal of this assessment is to determine whether ARPS-CANOPY can capture the vertical structure as well as the diurnal evolution of mean properties of the atmosphere in and above a canopy. Given the absence of evolving large-scale forcing, and the lack of any time-varying observed radiation input, what we are seeking to assess here is whether the model can achieve qualitative agreement with the observations, both in terms of the structure and evolution. The expectations of model accuracy must be tempered by the simplicity of the model experiment design as well as the intended application of ARPS-CANOPY. We remind the reader that our goal is to develop a smoke dispersion modeling system for simulating smoke transport from low-intensity fires. Thus, the absolute magnitude of mean wind, temperature, and TKE in the ambient environment are of lesser importance compared to the heat and turbulence induced by the fire.

In the absence of large-scale forcing, changes to the mean wind profiles will largely depend on turbulent mixing, which in turn is sensitive to vertical wind shear and strat-

©2013 This article is protected by copyright. All Rights Reserved.

ification. Thus, in seeking out the source of errors in the wind (and ultimately TKE) fields, it is important to evaluate possible sources of temperature error. Possible sources of error include uncertainty in the specification of the parameters in Eq. (5), uncertainty in the estimates of vegetation fraction, under-mixing by the ARPS model (by resolved and/or SGS eddies), and the use of time-invariant values of coefficients such as emissivity and extinction coefficient in Eq. (3) - (6) (since the variation of coefficients on diurnal and seasonal timescales is neglected). While the examination of these factors is ongoing, the sensitivity of model error to soil heat capacity and canopy albedo has been assessed. Variation of these parameters within the range of values observed during the CHATS field campaign result in small changes to mean temperature O(0.5 C) and mean wind speed O(0.25 m s^{-1}) (not shown).

Discrepancies between the simulations and observations may also result from documented inhomogeneities in the CHATS environment upwind of the tower which are not represented by the horizontally homogeneous canopy employed in the ARPS-CANOPY simulations. With respect to initialization error, it is unlikely that errors in the mean profiles (Figs. 3 and 4) result from errors in the initial state, as the data sources used to define the initial atmospheric profiles for the two cases (NARR, Sodar, wind profiler, 30-m tower) were in agreement regarding the primary aspects of the lower atmosphere (e.g., low-level jets, temperature inversions). Furthermore, the measurements of soil parameters (e.g., soil temperature) were quality controlled following the field campaign and all instruments were calibrated prior to deployment.

Comparing TKE between the model and CHATS tower observations (Fig. 5a-b), we see that in both cases the model replicates the overall profile shape throughout the rough-

Accepted Article

©2013 This article is protected by copyright. All Rights Reserved.

ness sub-layer. Regarding the magnitude of TKE, model error across the canopy-free atmosphere interface is found to be quite small, although larger differences are found elsewhere. Above the canopy, the model generates too much TKE in the pre leaf-out case, but underpredicts TKE in the post leaf-out case. The model errors noted above the canopy are likely due to overestimation of shear production in the pre leaf-out case, and underestimation in the post leaf-out case. For the pre leaf-out case, winds weaken too rapidly upon entering the canopy from above (simulated shear is too strong), while for the post leaf-out case, the model underpredicts wind speeds above the canopy (simulated shear is too weak) (cf. 1300-1600 LST mean in Figs. 3a and 4a). The underestimation of mean TKE in the post leaf-out case is likely also associated with the use of grid spacing that is too coarse to resolve some scales of turbulence at and above the canopy top [for a review of turbulent length scales observed during CHATS, see *Dupont and Patton*, 2012a]. In the lower half of the canopy, ARPS-CANOPY slightly overestimates TKE in both cases. Given the relatively small contribution of shear production to TKE in the lower portion of vegetation canopies [*Dwyer et al.*, 1997; *Finnigan*, 2000], the in-canopy model errors are likely due to canopy drag that is too weak and/or downward transport (pressure and/or turbulent) that is too strong. Examination of this potential model bias is left to future work. Finally, regarding the role of the SGS turbulence parameterization on total TKE, we see that in both cases the ratio of model SGS TKE to total TKE ranges from about 5% at the surface up to about 30% in the upper two-thirds of the canopy. Within several meters of the top of the canopy, the SGS TKE fraction reduces to 10% or less and decreases steadily upward.

Accepted Article

©2013 This article is protected by copyright. All Rights Reserved.

5.2. Model Evaluation: Radiation Analysis

With the assessment of mean and turbulent flow in the ARPS-CANOPY simulations complete, we now evaluate the simulation of net radiation at canopy top and at the ground surface. Figure 6 presents time series of net radiation from ARPS-CANOPY with CHATS observations overlaid; examination of the time series reveals a number of interesting features. First, the net radiation comparison at canopy top reveals model errors of roughly 20-30 W m^{-2}, with underprediction apparent in the pre leaf-out case and overprediction evident in the post leaf-out case. Although uncertainty exists with respect to the source of the error (e.g., albedo, emissivity, canopy temperature), the overall error is less than 5%. Second, with regards to net radiation at the bottom of the canopy, the ARPS-CANOPY ground net radiation time series are consistently within the upper range of the CHATS observations at 2 m AGL, with the observed data exhibiting larger variability. Such large variations in observed net radiation at the bottom of the CHATS orchard is most likely due to the change in position of the sun during the day and clumping of the canopy elements. This leads to net radiation at the canopy bottom varying between completely attenuated and completely unattenuated, with no perceivable pattern evident; such an effect is difficult to model. During the post leaf-out period of the CHATS campaign, long duration and large magnitude spikes in observed 2 m AGL net radiation are evident between 1000 and 1400 LST. The spikes suggest that instrument placement relative to the gap between rows of trees allows incoming solar radiation to reach the surface unattenuated for up to two hours (note that observed net radiation at 2 m AGL exceeds that at 16 m AGL due to greater downwelling longwave radiation beneath the canopy; not shown).

Accepted Article

©2013 This article is protected by copyright. All Rights Reserved.

Upon examining the ARPS-CANOPY simulated net radiation time series at canopy bottom, it is difficult to make the case that too much or too little attenuation of net radiation in Eq. (6) is the sole cause of the errors in simulated mean temperature evident in Figs. 3c and 4c. The model exhibited an afternoon warm bias in the pre leaf-out case and an afternoon cold bias in the post leaf-out case, yet an integration of the ground radiation time series reveals that in both cases too much energy reaches the ground in the simulations (not shown). Thus, it is more likely that factors such as inadequate SGS mixing and the use of constant coefficients (e.g., extinction coefficient) are to blame, and that further adjustment of model parameters would be necessary to yield a closer match to observations. However, it should be noted that in the pre leaf-out case, the ground net radiation computed in ARPS-CANOPY is too large and likely contributes to the model afternoon warm bias. The lack of measurements between 2 m and 16 m AGL, and uncertainty as to the representativeness of the CHATS near-ground radiation measurements, prevent a more complete assessment of ARPS-CANOPY net radiation.

5.3. Grid Structure Sensitivity Tests

Up to this point, the ARPS-CANOPY evaluation has focused solely on simulations from the inner domain, run with 30-m horizontal grid spacing. In this section, results from the outer domain simulation (90-m horizontal grid spacing) are examined in an effort to determine if simulations employing a horizontal grid spacing of O(100 m) can maintain the shape and diurnal trends of the mean and turbulent profiles seen in the inner domain simulations. Our primary goal here is to assess the impact of larger horizontal grid spacing on the ability of ARPS-CANOPY to resolve and/or parameterize turbulence, an ability that is highly dependent on grid cell dimensions. Since ARPS-CANOPY results with horizon-

Accepted Article

©2013 This article is protected by copyright. All Rights Reserved.

tal grid spacing O(100 m) can be produced in near-real time and employed to simulate smoke dispersion, it is desirable to assess model performance at this scale and determine whether differences introduced by the larger grid spacing could impact simulations of smoke dispersion. Thus, Figures 7, 8, and 9 are presented to compare mean profiles of wind, temperature and TKE from the outer domain simulations to corresponding profiles from the inner domain simulations (indicated by red lines in Figs. 7 - 9). Note that vertical grid structure is identical for all experiments discussed herein.

Examining the pre leaf-out case first (Figs. 7 and 9a), we find that with the exception of the first time period (0400-0700 LST), wind speeds in the outer domain simulation are approximately 0.5 m s^{-1} weaker on average in the roughness sub-layer, with the maximum difference occurring near canopy top; wind direction, however, exhibits little or no sensitivity. The weaker wind speeds in the outer domain simulation are the result of overall weaker downward mixing of high momentum during the development of the daytime mixed layer (not shown). As a result of changes to the mean wind speed profile, mean wind shear across the canopy interface is smaller in the outer domain simulation, while simultaneously larger above about twice canopy height (Fig. 7a). Thus, mean TKE above about z = 17.5 m is larger in the outer domain simulation, resulting in a small increase in TKE error compared to the inner domain simulation, with mean TKE below z = 17.5 m smaller in the outer domain simulation. The smaller mean TKE inside the canopy is consistent with the less-well-mixed temperature profiles and warmer surface temperatures in the outer domain simulation (Fig. 7c).

Assessment of the post leaf-out case outer domain simulation (Figs. 8 and 9b) reveals somewhat weaker winds above the canopy compared to the inner domain simulation;

©2013 This article is protected by copyright. All Rights Reserved.

however, unlike the pre leaf-out case, wind direction in the post leaf-out case shows greater sensitivity to grid structure, especially after 0700 LST. Interestingly, a more pronounced kink in the mean wind direction profile is seen in the outer domain simulation (Fig. 8b). Regarding temperature, less well-mixed temperature profiles are seen in the outer domain simulation, similar to the pre leaf-out case. The outer domain simulation yields smaller TKE throughout the roughness sub-layer, with differences between the outer and inner domain simulations largest above canopy top and restricted to approximately 20%.

At this point in the discussion, one might inquire as to why the horizontal grid spacing would be relevant here, since the flows we are simulating are horizontally homogeneous. In short, an increase in horizontal grid spacing from 30-m to 90-m yields a decrease in the amount of resolved TKE. The SGS turbulence closure we employ compensates for larger grid spacing via a grid-spacing-dependent eddy viscosity, but the identical vertical grid structure applied in both the fine and coarse horizontal grid spacing runs results in similar amounts of SGS TKE since turbulence production is highly sensitive to the model's ability to resolve vertical gradients of wind and temperature. Thus, the strength of turbulent mixing (resolved and SGS combined) varies between runs with 30- and 90-m horizontal grid spacing, and the profiles of mean wind and temperature differ.

The different mean profiles exhibited by simulations with 90-m and 30-m horizontal grid spacing lead one to question whether the larger horizontal grid spacing is adequate for simulating smoke dispersion from low-intensity fires. We address this question in two wind and turbulence regimes: the first regime has a stronger mean wind and larger TKE (pre leaf-out, 29 March 2007); the second regime has a weaker mean wind and smaller TKE (post leaf-out, 20 May 2007). Note that in both regimes, the larger horizontal

Accepted Article

©2013 This article is protected by copyright. All Rights Reserved.

grid spacing contributes to generally smaller TKE and weaker mean wind speeds in the roughness sub-layer. Consistent with reduced TKE in the lowest 15-20 m AGL in the 90-m horizontal grid spacing simulations, mean temperature profiles were less well-mixed and surface temperatures were about 2 ^{o}C warmer during the afternoon. The primary difference between the two cases occurs in the simulated wind direction: in the pre leaf-out case, mean wind direction was unaffected by grid resolution, while for the post leaf-out case mean wind direction was found to be sensitive to the grid structure. However, since roughness-layer mean wind speeds in the post leaf-out case are generally quite weak (less than 2.5 m s^{-1}), the impact of this grid sensitivity on smoke dispersion simulations would be reduced.

These results reveal that in both cases wind speed, TKE, and temperature are influenced by grid resolution, while sensitivity of wind direction to grid structure is limited to the weak wind case (post leaf-out). The larger horizontal grid spacing does not degrade the mean profile shape and diurnal trends from the higher-resolution simulation. Since the near-real time application of ARPS-CANOPY requires horizontal grid spacing of O(100 m), these results suggest that a near real-time smoke prediction system can be developed and applied, with the limitations noted herein.

6. Summary and Conclusions

The development and evaluation of a new integrated canopy flow modeling system developed from the ARPS model, termed ARPS-CANOPY, has been presented. The standard ARPS model has been modified to account for the effect of vegetation elements on mean and turbulent flow and on the net radiation flux profiles within the canopy. Improving the understanding of smoke transport from low-intensity fires and developing

©2013 This article is protected by copyright. All Rights Reserved.

Accepted Article

operational modeling tools for predicting smoke dispersion within and in the vicinity of forest vegetation layers provide the motivation for these efforts. As an important step in the model development process, the atmospheric model has been evaluated using data from the CHATS experiment. Comparisons of mean and turbulent flow properties have been presented for two cases, one prior to and one following leaf-out, and sensitivity of results to grid structure have been examined.

In both cases, ARPS-CANOPY was shown to underestimate the mean wind speed in the hours following model initialization. Given the lack of evolving large-scale forcing in the simulations, discrepancies between observed and model profiles are expected, particularly with respect to the wind. However, the model was shown to reproduce the observed shape and magnitude of the wind speed profiles during the late morning through late afternoon period in the pre leaf-out case and reproduce the profile shape in the (light-wind) post leaf-out case. In the case of wind direction, the model correctly maintained a nearly uniform profile in the pre leaf-out case and successfully captured the observed kink in the wind direction profile during the morning in the post leaf-out case. Regarding temperature, model errors of opposite sign were noted in the pre and post leaf-out cases, indicating that further adjustment of model parameters (e.g., extinction coefficient) would be necessary to achieve a closer match to observations. The model was shown in both cases to overestimate TKE inside the lower canopy, and in the pre leaf-out case also overestimate TKE above the canopy; however, profile shape was similar to observations. Sensitivity experiments with relatively coarse 90-m horizontal grid spacing were shown to retain the overall mean profile shape and diurnal trends seen in the finer-resolution simulations.

Accepted Article

©2013 This article is protected by copyright. All Rights Reserved.

Despite the qualitative agreement with the CHATS observations, further efforts are required to attain closer agreement with observations. Future efforts planned include performing sensitivity tests with canopy parameters we have identified herein as primary sources of uncertainty, and performing heat, momentum, and turbulence budget analyses to examine the sources of error. Specific parameters to be examined include Bowen ratio (incorporating diurnal variation), extinction coefficient (using CHATS radiation measurements to compute case-specific extinction coefficients), and volumetric heat capacity (adjusting the parameter as in *Froelich et al.* [2011]). However, it needs to be emphasized here that our goal is to develop a smoke dispersion modeling system for simulating smoke transport from low-intensity fires. Thus, the absolute magnitude of temperature and TKE in the ambient environment are of lesser importance compared to the heat and turbulence induced by the fire.

We conclude by emphasizing the advancement of the model from its former state to the current one: it is now possible to simulate airflow beneath canopy top under non-neutral conditions with ARPS, which is critical for predicting the local transport and diffusion of wildland fire smoke in forested environments. The work presented herein and the suggested future work are part of a larger effort to design a smoke management tool specifically applicable to low-intensity fires. The operational need for such a prediction tool motivates all of these efforts.

Acknowledgments. We wish to thank Jehan Rihani and three anonymous reviewers for their helpful comments and suggestions regarding the manuscript. Support for this research was provided by the U.S. Joint Fire Science Program (Project # 09-1-04-1) and the USDA Forest Service (Research Joint Venture Agreement # 09-JV-11242306-089).

©2013 This article is protected by copyright. All Rights Reserved.

Accepted Article

References

Andreae, M. O., P. Artaxo, C. Brandão, F. E. Carswell, P. Ciccioli, A. L. da Costa, A. D. Culf, J. L. Esteves, J. H. C. Gash, J. Grace, P. Kabat, J. Lelieveld, Y. Malhi, A. O. Manzi, F. X. Meixner, A. D. Nobre, C. Nobre, M. d. L. P. Ruivo, M. A. Silva-Dias, P. Stefani, R. Valentini, J. von Jouanne, and M. J. Waterloo (2002), Biogeochemical cycling of carbon, water, energy, trace gases, and aerosols in Amazonia: The LBA-EUSTACH experiments, *J. Geophys. Res.*, *107*(D20), 8066, doi:10.1029/2001JD000524.

Aumond, P., V. Masson, C. Lac, B. Gauvreau, S. Dupont, and M. Berengier (2013), Including the drag effects of canopies: Real case large-eddy simulation studies, *Boundary-Layer Meteorol.*, *146*, 65–80.

Ayotte, K. W., J. J. Finnigan, and M. R. Raupach (1999), A second-order closure for neutrally stratified vegetative canopy flows, *Boundary-Layer Meteorol.*, *90*, 189–216.

Borel, C. C., S. A. W. Gerstl, and B. J. Powers (1991), The radiosity method in optical remote sensing of structure 3-d surfaces, *Remote Sens. Environ.*, *36*, 13–41.

Budagovskii, A. I., J. K. Ross, and H. G. Tooming (1968), Distribution of the long-wave radiation fluxes and the radiation balance in plant cover, in *Actinometry and Atmospheric Optics: Proceedings of the Sixth Interdepartmental Symposium on Actinometry and Atmospheric Optics*, pp. 287–296.

Chelle, M., and B. Andrieu (1998), The nested radiosity model for the distribution of light within plant canopies, *Ecol. Model.*, *111*, 75–91.

Chou, M.-D. (1990), Parameterization for the absorption of solar radiation by O_2 and CO_2 with application to climate studies, *J. Clim.*, *3*, 209–217.

Accepted Article

©2013 This article is protected by copyright. All Rights Reserved.

Chou, M.-D. (1992), A solar radiation model for climate studies, *J. Atmos. Sci.*, *49*, 762–772.

Chou, M.-D., and M. J. Suarez (1994), An efficient thermal infrared radiation parameterization for use in general circulation models, *Tech. Rep. NASA Tech. Memo 104606*, [Available from NASA Center for Aerospace Information, 800 Elkridge Landing Road, Linthicum Heights, MD 21090-2934].

Dupont, S., and Y. Brunet (2008), Influence of foliar density profile on canopy flow: A large-eddy simulation study, *Agric. For. Meteorol.*, *148*, 976–990.

Dupont, S., and E. G. Patton (2012a), Influence of stability and seasonal canopy changes on micrometeorology within and above an orchard canopy: The CHATS experiment, *Agric. For. Meteorol.*, *157*, 11–29.

Dupont, S., and E. G. Patton (2012b), Momentum and scalar transport within a vegetation canopy following atmospheric stability and seasonal canopy changes: The CHATS experiment, *Atmos. Chem. Phys.*, *12*, 5913–5935.

Dwyer, M. J., E. G. Patton, and R. H. Shaw (1997), Turbulent kinetic energy budgets from a large eddy simulation of airflow above and within a forest canopy, *Boundary-Layer Meteorol.*, *84*, 23–43.

Finnigan, J. J. (2000), Turbulence in plant canopies, *Annu. Rev. Fluid Mech.*, *32*, 519–571.

Froelich, N. J., C. S. B. Grimmond, and H. P. Schmid (2011), Nocturnal cooling below a forest canopy: Model and evaluation, *Agric. For. Meteorol.*, *151*, 957–968.

Garai, A., J. Kleissl, and S. G. Llewellyn Smith (2010), Estimation of biomass heat storage using thermal infrared imagery: Application to a walnut orchard, *Boundary-Layer Meteorol.*, *137*, 333–342.

Accepted Article

©2013 This article is protected by copyright. All Rights Reserved.

Kanda, M., and M. Hino (1994), Organized structures in developing turbulent flow within and above a plant canopy, using a large eddy simulation, *Boundary-Layer Meteorol.*, *68*, 237–257.

Kimes, D. S., J. A. Smith, and L. E. Link (1981), Thermal IR exitance model of a plant canopy, *Appl. Optics*, *20*, 623–632.

Larkin, N. K., S. M. O'Neill, R. Solomon, S. Raffuse, T. Strand, D. C. Sullivan, C. Krull, M. Rorig, J. L. Peterson, and S. A. Ferguson (2009), The BlueSky smoke modeling framework, *Int. J. Wildland Fire*, *18*, 906–920.

Lavdas, L. (1996), Program VSMOKE - User's manual, *Tech. Rep. USDA Forest Service, Gen. Tech. Report SRS-6.*

Mason, P. J. (1994), Large-eddy simulation: A critical review of the technique, *Q. J. R. Meteorolog. Soc.*, *120*, 1–26.

Mesinger, F., G. DiMego, E. Kalnay, K. Mitchell, P. C. Shafran, W. Ebisuzaki, D. Jovic, J. Woollen, E. Rogers, E. H. Berbery, M. B. Ek, Y. Fan, R. Grumbine, W. Higgins, H. Li, Y. Lin, G. Manikin, D. Parrish, and W. Shi (2006), North American Regional Reanalysis, *Bull. Am. Meteorol. Soc.*, *87*, 343–360.

Noilhan, J., and S. Planton (1989), A simple parameterization of land surface processes for meteorological models, *Mon. Weather Rev.*, *117*, 536–549.

Patton, E. G., T. W. Horst, P. P. Sullivan, D. H. Lenschow, S. P. Oncley, W. O. J. Brown, S. P. Burns, A. B. Guenther, A. Held, T. Karl, S. D. Mayor, L. V. Rizzo, S. M. Spuler, J. Sun, A. A. Turnipseed, E. J. Allwine, S. L. Edburg, B. K. Lamb, R. Avissar, R. J. Calhoun, J. Kleissl, W. J. Massman, K. T. Paw U, and J. C. Weil (2011), The canopy horizontal array turbulence study (CHATS), *Bull. Am. Meteorol. Soc.*, *92*, 593–611.

Accepted Article

©2013 This article is protected by copyright. All Rights Reserved.

Pinard, J. D. J.-P., and J. D. Wilson (2001), First- and second-order closure models for wind in a plant canopy, *J. Appl. Meteorol.*, *40*, 1762–1768.

Pleim, J. E., and A. Xiu (1995), Development and testing of a surface flux and planetary boundary layer model for application in mesoscale models, *J. Appl. Meteorol.*, *34*, 16–32.

Raupach, M., and A. Thom (1981), Turbulence in and above plant canopies, *Annu. Rev. Fluid Mech.*, *13*, 97–129.

Riebau, A. R., D. G. Fox, M. L. Sestak, B. Dailey, and S. F. Archer (1988), Simple approach smoke estimation model, *Atmos. Environ.*, *22*, 783–788.

Ross, A. N., and S. B. Vosper (2005), Neutral turbulent flow over forested hills, *Q. J. R. Meteorolog. Soc.*, *131*, 1841–1862.

Rudnicki, M., S. J. Mitchell, and M. D. Novak (2004), Wind tunnel measurements of crown streamlining and drag relationships for three conifer species, *Can. J. For. Res.*, *34*, 666–676.

Shaw, R. H., and E. G. Patton (2003), Canopy element influences on resolved- and subgrid-scale energy within a large-eddy simulation, *Agric. For. Meteorol.*, *115*, 5–17.

Shaw, R. H., and U. Schumann (1992), Large-eddy simulation of turbulent flow above and within a forest, *Boundary-Layer Meteorol.*, *61*, 47–64.

Shen, S., and M. Y. Leclerc (1997), Modeling the turbulence structure in the canopy layer, *Agric. For. Meteorol.*, *87*, 3–25.

Smith, J. A., K. J. Ranson, D. Nguyen, L. Balick, L. E. Link, L. Fritschen, and B. Hutchison (1981), Thermal vegetation canopy model studies, *Remote Sens. Environ.*, *11*, 311–326.

Accepted Article

©2013 This article is protected by copyright. All Rights Reserved.

Smith, J. A., J. R. Ballard Jr., and J. A. Pedelty (1997), Effect of three-dimensional canopy architecture on thermal infrared exitance, *Optical Eng.*, *36*, 3093–3100.

Sogachev, A., G. V. Menzhulin, M. Heimann, and J. Lloyd (2002), A simple three-dimensional canopy - planetary boundary layer simulation model for scalar concentrations and fluxes, *Tellus*, *54B*, 784–819.

Sun, H., T. L. Clark, R. B. Stull, and T. A. Black (2006), Two-dimensional simulation of airflow and carbon dioxide transport over a forested mountain. Part I: Interactions between thermally-forced circulations, *Agric. For. Meteorol.*, *140*, 338–351.

Uchijima, Z. (1961), On characteristics of heat balance of water layer under paddy plant cover, *Bull. Nat. Inst. Agric. Sci., Ser. A*, *8*, 243–263.

Utiyama, M., T. Fukuyama, Y. Y. Maruo, T. Ichino, K. Izumi, H. Hara, K. Takano, H. Suzuki, and M. Aoki (2004), Formation and deposition of ozone in a red pine forest, *Water, Air, and Soil Pollut.*, *151*, 53–70.

Watanabe, T. (2004), Large-eddy simulation of coherent turbulence structures associated with scalar ramps over plant canopies, *Boundary-Layer Meteorol.*, *112*, 307–341.

Wilson, N. R., and R. H. Shaw (1977), A higher order closure model for canopy flow, *J. Appl. Meteorol.*, *16*, 1197–1205.

Xue, M., K. K. Droegemeier, and V. Wong (2000), The Advanced Regional Prediction System (ARPS) – A multi-scale nonhydrostatic atmosphere simulation and prediction model. Part I: Model dynamics and verification, *Meteorol. Atmos. Phys.*, *75*, 463–485.

Xue, M., K. K. Droegemeier, V. Wong, A. Shapiro, K. Brewster, F. Carr, D. Weber, Y. Liu, and D. Wang (2001), The Advanced Regional Prediction System (ARPS) – A multi-scale nonhydrostatic atmosphere simulation and prediction tool. Part II: Model

Accepted Article

©2013 This article is protected by copyright. All Rights Reserved.

physics and applications, *Meteorol. Atmos. Phys.*, *76*, 143–165.

Xue, M., D. Wang, J. Gao, K. Brewster, and K. K. Droegemeier (2003), The Advanced Regional Prediction System (ARPS), storm-scale numerical weather prediction and data assimilation, *Meteorol. Atmos. Phys.*, *82*, 139–170.

Yamada, T. (1982), A numerical study of turbulent airflow in and above a forest canopy, *J. Meteorol. Soc. Jpn.*, *60*, 439–454.

Accepted Article

©2013 This article is protected by copyright. All Rights Reserved.

Accepted Article

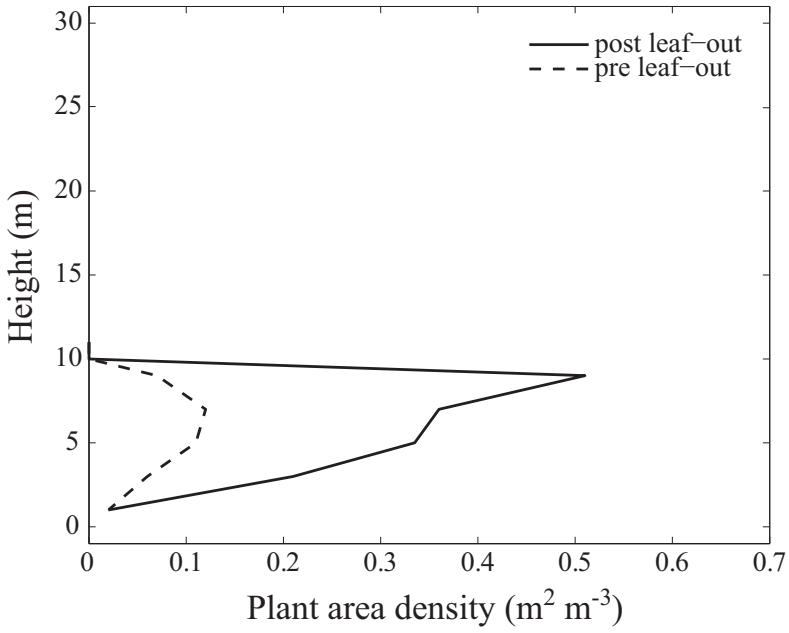

Figure 1. Vertical profiles of plant area density observed during the CHATS experiment, interpolated to the model grid.

©2013 This article is protected by copyright. All Rights Reserved.

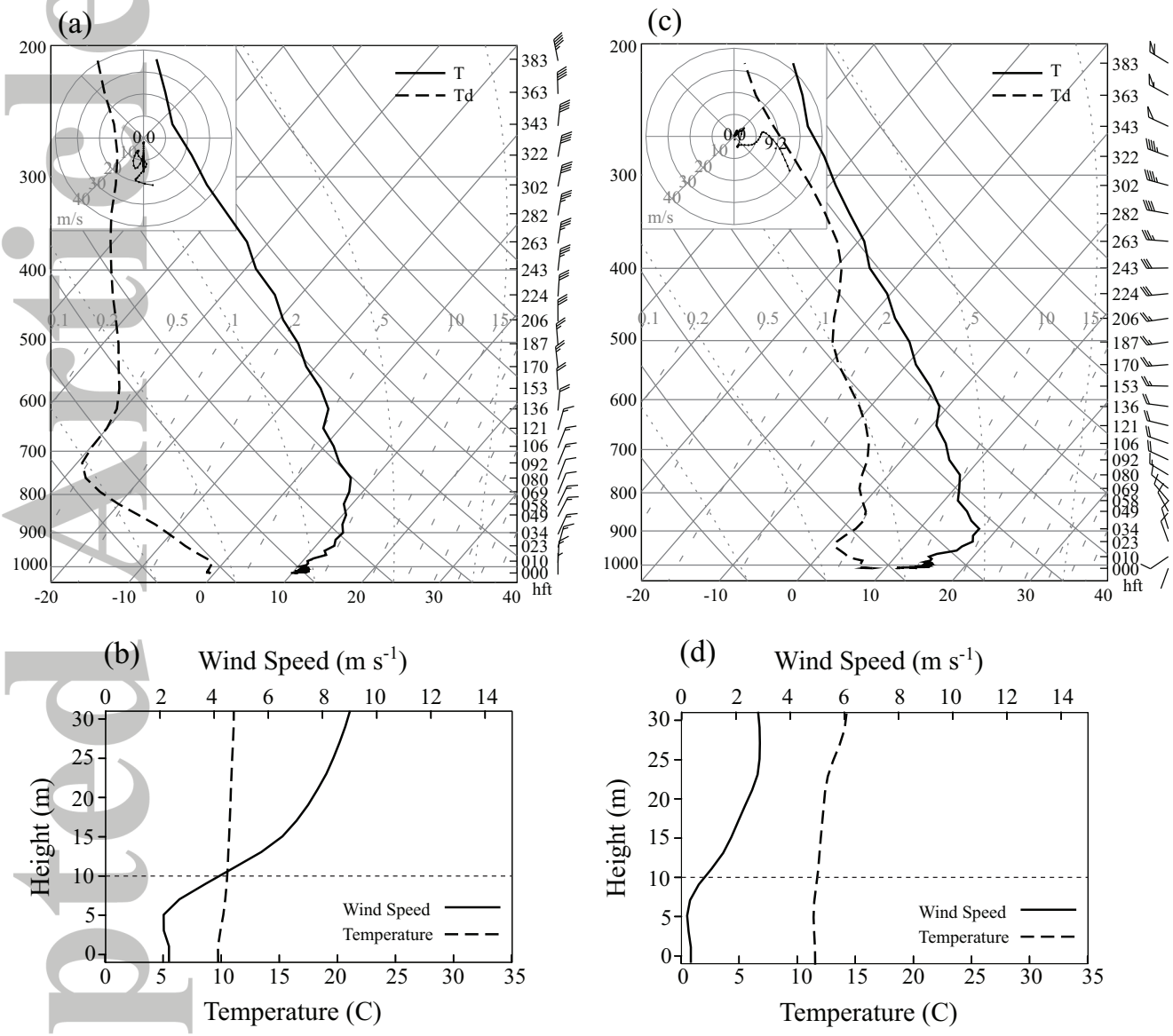

Figure 2. Initial state used to initialize ARPS-CANOPY: (a,c) SkewT–Log$p$ diagrams covering entire vertical depth of model, (b,d) profiles of temperature and wind speed across lowest 30 m of model atmosphere. Left-hand panels correspond to the pre leaf-out case (March 29), and right-hand panels correspond to the post leaf-out case (May 20). Horizontal dashed line in (b,d) denotes the canopy top. See text for description of methodology used to generate initial state.

Accepted Article

©2013 This article is protected by copyright. All Rights Reserved.

Accepted Article

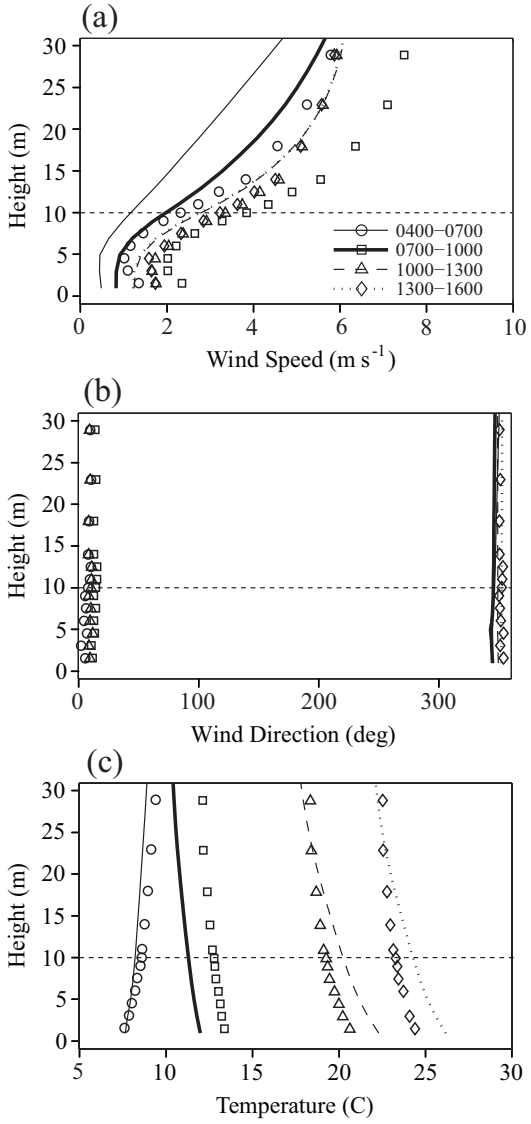

Figure 3. Comparison of simulated pre leaf-out (29 March 2007) mean (a) wind speed, (b) wind direction, and (c) temperature to values measured during the CHATS experiment, from the inner domain simulation. Line profiles are from the ARPS-CANOPY simulation and symbols denote the observed values; legend in (a) applies to all panels. Both simulated and measured hourly wind speeds are averaged over four 3-hour windows, with the simulated data also averaged spatially over the entire inner domain. Times in legend are in Local Standard Time (LST: UTC-8). Horizontal dashed line denotes the canopy top.

©2013 This article is protected by copyright. All Rights Reserved.

Accepted Article

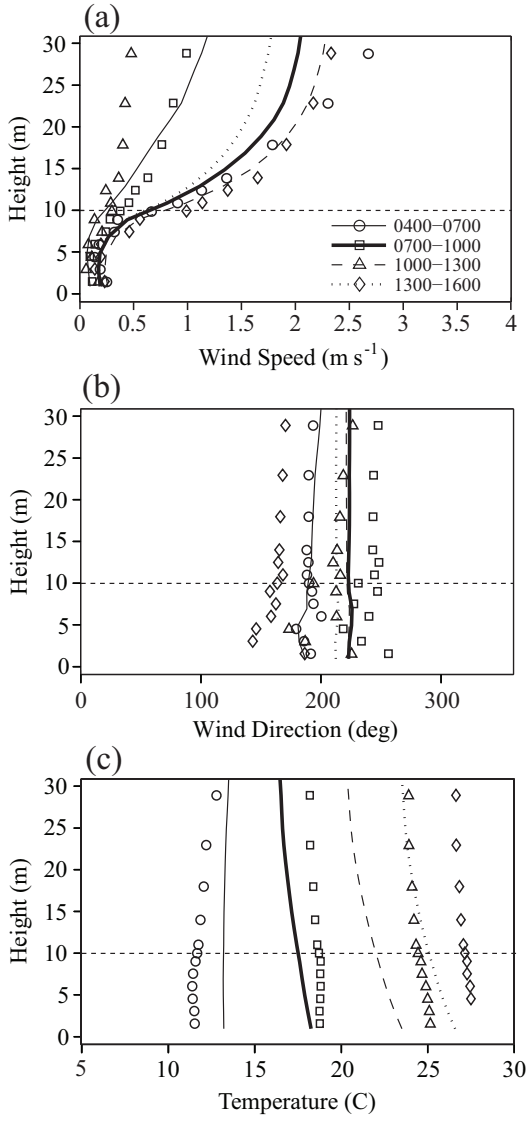

Figure 4. As in Fig. 3, but for the post leaf-out case (20 May 2007). Note the change in horizontal axis limits for (a).

©2013 This article is protected by copyright. All Rights Reserved.

Accepted Article

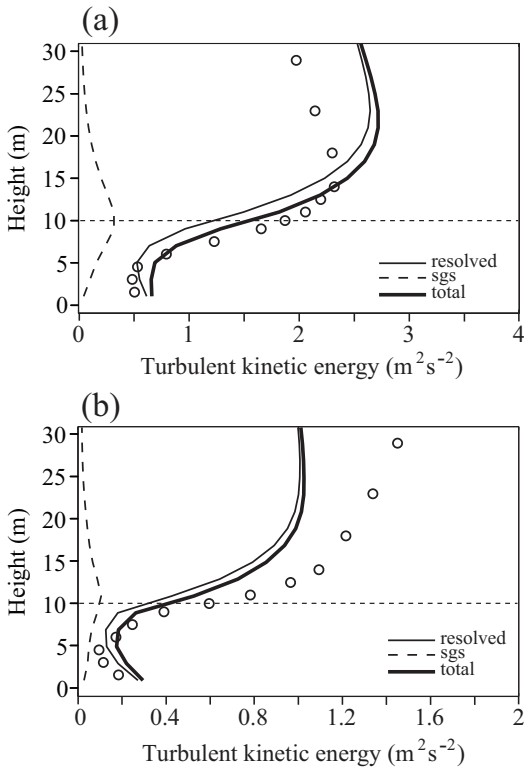

Figure 5. 1300-1500 LST mean vertical profiles of ARPS-CANOPY simulated TKE, for the (a) pre leaf-out case and (b) post leaf-out case, from the inner domain simulation. CHATS observations are indicated by symbols. Horizontal dashed line denotes the canopy top. Simulated profiles are computed starting with a two-hour block of model output at 1Hz frequency, with perturbations computed from 30-minute means. Turbulent statistics are then computed, and subsequently averaged horizontally across the model domain, and across the four 30-minute time blocks. The observed TKE was computed using 5-minute averaging periods which were subsequently combined to produce 30-minute average statistics (see Section 3 for description of method used). Note difference in horizontal axis limits between panels.

©2013 This article is protected by copyright. All Rights Reserved.

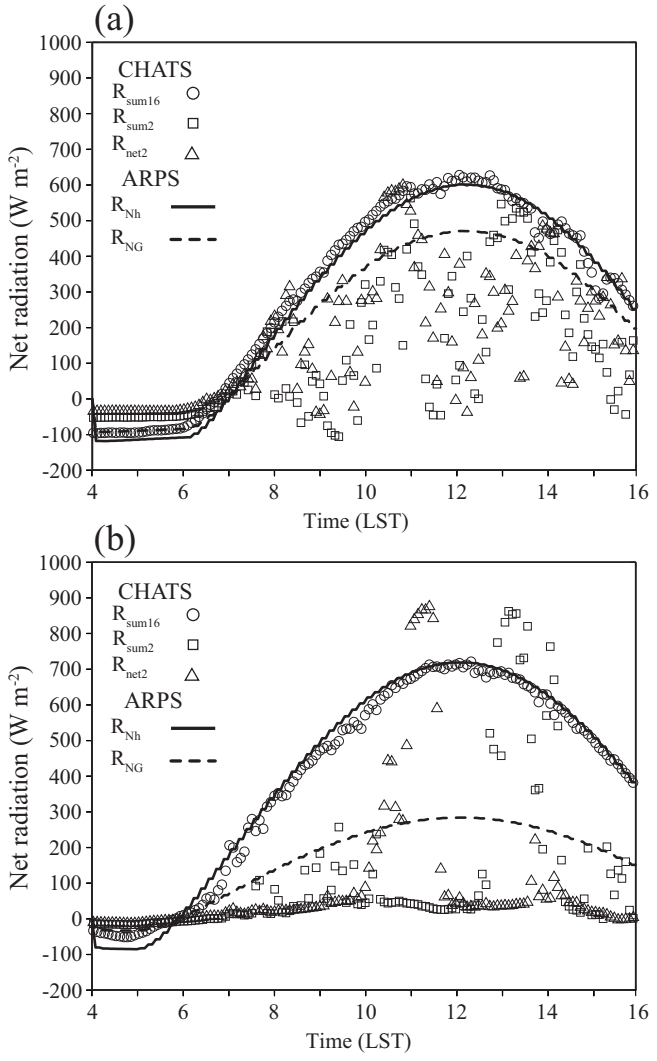

Figure 6. Time series of net radiation at various levels of the canopy, for the (a) pre leaf-out and (b) post leaf-out cases. Lines represent model domain mean ARPS-CANOPY simulation data and symbols indicate 5-min mean CHATS observations (see legend). For CHATS observations, R_{sum} is the sum of the radiation components measured by a system of pyranometers and pyrgeometers (4-component radiometer) deployed during the field experiment, while R_{net} is the net radiation measured by a 1-component net radiometer. For ARPS-CANOPY results, R_{Nh} is the net radiation at canopy top [Eq. (3)] and R_{NG} is the net radiation computed at the ground [Eq. (6)]. The subscript number indicates height above ground level.

Accepted Article

©2013 This article is protected by copyright. All Rights Reserved.

Accepted Article

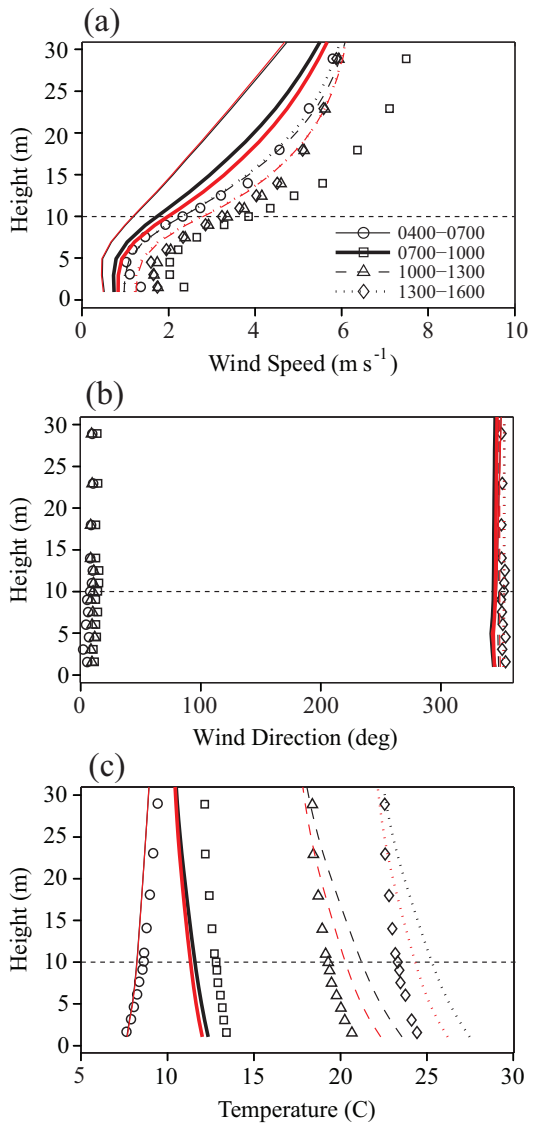

Figure 7. As in Fig. 3, but for the outer domain simulation. The inner domain simulation profiles are overlaid with red lines.

©2013 This article is protected by copyright. All Rights Reserved.

Accepted Article

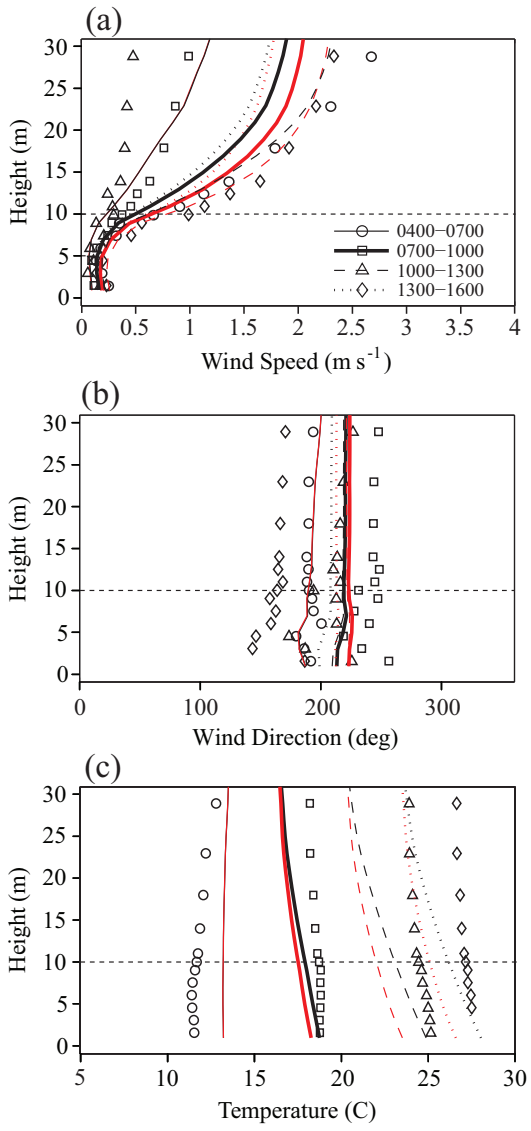

Figure 8. As in Fig. 4, but for the outer domain simulation. The inner domain simulation profiles are overlaid with red lines.

©2013 This article is protected by copyright. All Rights Reserved.

Accepted Article

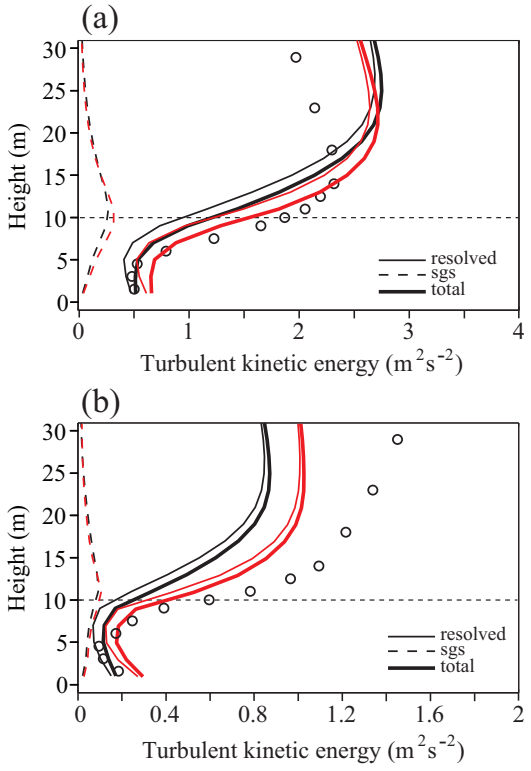

Figure 9. As in Fig. 5, but for the outer domain simulation. The inner domain simulation profiles are overlaid with red lines.

©2013 This article is protected by copyright. All Rights Reserved.